Regional moment tensor inversion using rotational observations

Gene Ichinose[1], Sean Ford[1], and Robert Mellors[1]

[1]Lawrence Livermore National Laboratory

November 23, 2022

Abstract

There are potential benefits from the addition of 3-C rotational motions to traditional 3-C translational displacements for moment tensor (MT) inversions. The rotational radiation pattern is orthogonal to the shear radiation pattern, thus incorporating rotations is equivalent to gaining another observation point on the focal sphere. We demonstrate this by simulating the curl and displacement wavefields in a half-space for a regional distance station. We also demonstrate the effect of velocity gradients beneath a station on rotational motions compared to displacements. Further investigation is needed to study how this affects the MT inversion. We added rotational Greens functions to regional long-period MT inversion computing spatial gradients from f-? reflectivity synthetics. We used array derived rotational motions from the Piñon Flats Observatory Array in California and Golay arrays deployed during the IRIS Community Wavefield Demonstration Experiment in Oklahoma. Well-constrained MT solutions were estimated for three earthquakes using long-period regional waves with and without rotational ground motions as test cases. Prepared by LLNL under Contract DE-AC52-07NA27344. This work was performed under the auspices of the U.S. Department of Energy by Lawrence Livermore National Laboratory under Contract DE-AC52-07NA27344. LLNL release number LLNL-ABS-781439. Index Terms: 7215 Earthquake source observations, 7290 Computational seismology Plain-Language Summary Scientists have traditionally used seismometers to record earthquake generated translational ground motions using three-dimensional axes typically oriented in a vertical, north-south and east-west directions in other words a “Cartesian coordinate system”. Recent advancements in seismometer development for recording rotational or twisting ground motions about the same three-axes provide additional information, which, in addition to translational seismometers can help resolve the radiation patterns of quakes. In cases where physical access is limited, the sparse distribution of seismometers caused by, for example, ocean coasts, islands, Lunar, and Mars surfaces can prevent the complete observation of the quake radiation pattern. The combination of these two types of seismometers at a single point are useful to infer faulting mechanisms of quakes or other seismic source types than using just one seismometer. Submitted to American Geophysical Union Fall Meeting, San Francisco, CA 9-13 December 2019. S032 – Rotation and Strain in Seismology – Applications, Instrumentation and Theory S21G-0589

Lawrence Livermore National Laboratory

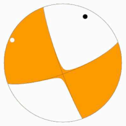

American Geophysical Union Fall Meeting, San Francisco, CA 9-13 December 2019. S032 – Rotation and Strain in Seismology – Applications, Instrumentation and Theory. Tuesday 10 Dec 2019 08:00-12:00 S21G-0589

Regional Moment Tensor Inversion using Rotational Observations

Gene A. Ichinose, Sean R. Ford and Robert J. Mellors

Lawrence Livermore National Laboratory

This work was performed under the auspices of the US Department of Energy by Lawrence Livermore National Laboratory under contract DE-AC52-07NA27344. Release #LLNL-POST-798406

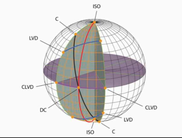

AEED

Introduction / Summary

1. We use the simplest approach to calculate rotational Greens functions for incorporating into regional moment tensor (MT) inversions (see section 2).
2. We did not have three-component (3-C) rotational data "yet" so we used array-derived rotations from the Pinon Flat Observatory in California and Golay array in Enid, Oklahoma. We successfully demonstrate inclusion of 3-C rotational with 3-C translational data into MTINV version 4.0.0 [*https://sourceforge.net/projects/mtinv/*] (see section 3).
3. We examined the sensitivity of Full-MT solutions by including 3-C rotational data with regular translational displacement data using Network Sensitivity Solution (NSS) approach by plotting the percent variance reduction on Eigenvalue sphere or Lune (see section 4).
4. The examples of two and three-station 3-C datasets with 3-C rotational data improved the MT solution sensitivity, by increasing Double-Couple (DC) components and reducing Compensated Linear Vector Dipole (CLVD) and isotropic (ISO) components relative to using just the 3-C translational displacement data alone (see section 4).

Motivation: Donner et al. (2016) published a paper titled, "*Inversion for seismic moment tensors combining translational and rotational ground motions.*" Their encouraging study is based on synthetic scenarios and states: "*Our results indicate that the resolution of the moment tensor can be increased drastically by incorporating rotational ground motion data. Especially, the usually problematic components Mxz and Myz as well as all components containing spatial derivatives with depth...*"

1. Exploring Rotational and Displacement Synthetics and Radiation Patterns using a Gradient 3-D Velocity Model

1.1) The displacement radiation patterns are provided by Aki and Richards (2002) Equation 4.33 and the far-field *S* is:

$$\boldsymbol{AFS} = \cos(2\theta)\cos(\phi)\hat{\boldsymbol{\theta}} - \cos(\theta)\sin(2\phi)\hat{\boldsymbol{\phi}},$$

where $\hat{\boldsymbol{\theta}}$ and $\hat{\boldsymbol{\phi}}$ are the unit vectors in the spherical coordinate system (shown in Aki and Richards (2002) Figure 4.4). The rotation radiation pattern is provided by Cochard et al. (2006) Equation 30.4. The far-field rotation is a function of the derivative of the moment-rate function and its radiation pattern is:

$$\boldsymbol{AR} = \cos(\theta)\sin(\phi)\hat{\boldsymbol{\theta}} + \cos(2\theta)\sin(\phi)\hat{\boldsymbol{\phi}}.$$

1.2) As Cochard et al. (2006) concludes, the rotation radiation pattern *AR* can be obtained from shear radiation pattern *AFS* by $\nabla \times \boldsymbol{AFS} = \boldsymbol{AR}/r$, and therefore the far-field shear radiation pattern is orthogonal to the far-field rotation pattern.

1.3) Thus, one six-component (6-C) station can gather the same information on radiation pattern as two three-component (3-C) stations at 90° azimuth from one another along the focal plane axis, which is sometimes difficult to obtain when restricted to surface sensors. Additionally, information on the derivative of the moment-rate function can be obtained in the far-field, which would provide a constraint on the source-time function, though not in the case of long-period moment tensors, where the source-time function is taken as a step (or moment-rate delta). We demonstrate the difference in the wavefield by simulating the displacements and rotations at a distance of 100 km from a M 5 normal faulting (strike = 33°, rake = –76°, dip = 50°) earthquake (Brune (1970) source displacement with 1-sec rise-time) at a depth of 10 km.

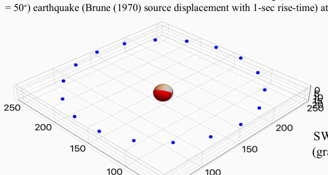

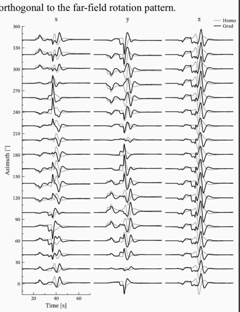

SW4 simulation comparison of displacement for the homogeneous (gray) and gradient (black) medium for the velocity profiles shown below. The gradient synthetics are shifted by 3-seconds.

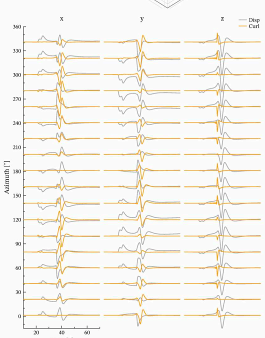

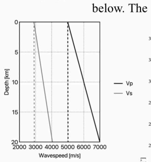

SW4 simulations of displacement (gray) and rotation (orange) for a constant velocity half-space (α = 5000 m/s, β = 2900 m/s and ρ = 2650 kg/m3)1. The rotation (curl) is multiplied by a factor of 1000.

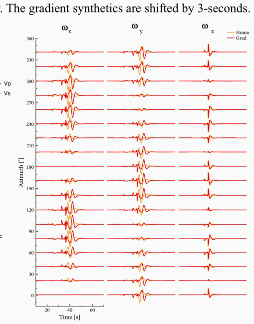

SW4 simulation comparison of rotation for the homogeneous (orange) and gradient (red) medium for the velocity profiles shown above. The gradient synthetics are shifted by 3-seconds.

SW4: https://computing.llnl.gov/projects/serpentine-wave-propagation

3. Waveform Data and Deviatoric Moment Tensor Inversion Results: Broadband 3-C Arrays and 3-C Single Stations

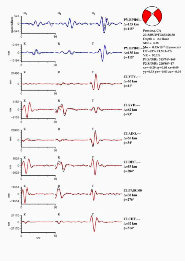

Piñon Flat Observatory Array

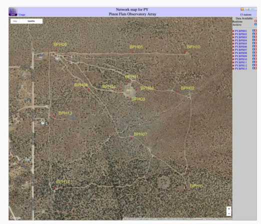

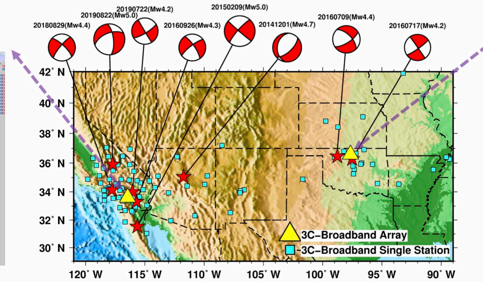

Broadband Golay Array

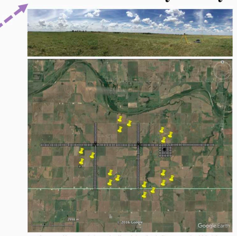

https://www.iris.edu/hq/site/PAGE_static/4261

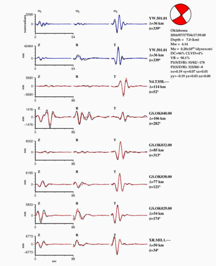

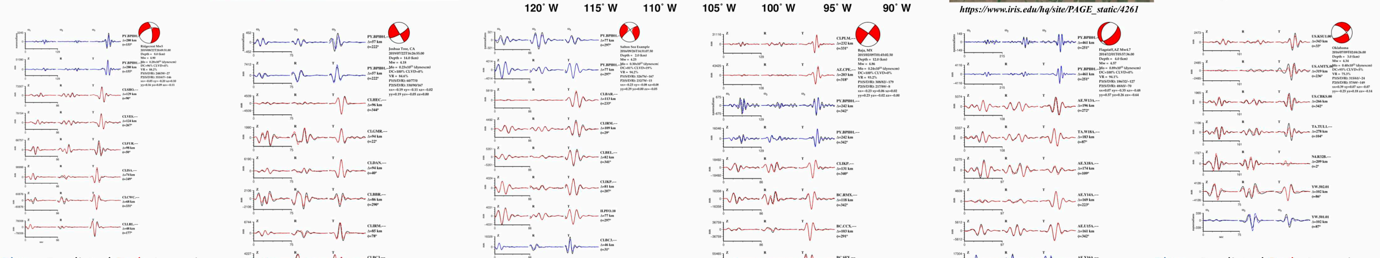

Blue – Predicted Red - Inversion

Blue – Predicted Red - Inversion

2. Methods: Computing Rotational Green Functions for MT Inversion

- Rotational motions computed using 5-point stencil.
  - GFs are computed at 4 points around center reference point (see right) for each fundament faulting orientation (**SS**, **DS**, **DD)** and isotropic GFs.
  - Spatial gradient computed using 2-point finite difference along the X- and Y-axes
  - Rotate 3-components from vertical, radial, transverse (z,r,t) to vertical, north, east (z,n,e) coordinates

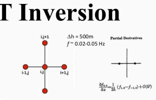

- Associate the component of rotation to P-SV or SH radiation patterns (e.g., Benioff & Gutenberg, 1952, Pascal & Muyzert, 2013; Li & Baan, 2017)
  - $\vec{\omega}$= rotation rate vector
  - $\vec{p}$= slowness vector (x-radial, y-tangental, z-vertical)
  - $\vec{u}$= displacement
  - $\dot{\omega}_x \sim p_x \cdot \ddot{u}_z$
  - $\dot{\omega}_y \sim p_y \cdot \ddot{u}_z$
  - $\dot{\omega}_z = -\frac{1}{2} p_z \cdot \ddot{u}_y$
  - The rotation about the x and y axes should scale with vertical component and therefore have a P-SV radiation pattern.
  - The rotation about the z axes scales with the tangential component and therefore has the SH-wave radiation pattern.

$$\begin{pmatrix}\omega_x\\ \omega_y\\ \omega_z\end{pmatrix} = \frac{1}{2}\begin{pmatrix}\partial_x\\ \partial_y\\ \partial_z\end{pmatrix} \times \begin{pmatrix}u_x\\ u_y\\ u_z\end{pmatrix} = \frac{1}{2}\begin{pmatrix}\partial_y u_z - \partial_z u_y\\ \partial_z u_x - \partial_x u_z\\ \partial_x u_y - \partial_y u_x\end{pmatrix},$$

$$\omega_x = \frac{\partial u_z}{\partial x_y}; \quad \omega_y = \frac{\partial u_z}{\partial x_x}; \quad \omega_z = \frac{1}{2}\left(\frac{\partial u_x}{\partial x_y} - \frac{\partial u_y}{\partial x_x}\right);$$

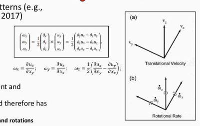

Free Surface Effects – strain and rotations

Zero traction boundary condition at free surface implies that $(\sigma_{i,z} = 0\ (i = x, y, z))$. Hooke's law $\sigma_{ij} = \lambda\epsilon_{kk}\delta_{ij} + 2\mu\epsilon_{ij}$ in homogeneous isotropic medium leads to:

$$\frac{\partial u_x}{\partial x_z} = -\frac{\partial u_z}{\partial x_x}; \quad \frac{\partial u_y}{\partial x_z} = -\frac{\partial u_z}{\partial x_y}; \quad \frac{\partial u_z}{\partial x_z} = -\frac{\lambda}{\lambda + 2\mu}\left(\frac{\partial u_x}{\partial x_x} + \frac{\partial u_y}{\partial x_y}\right)$$

$$\vec{\boldsymbol{\omega}} = \frac{1}{2}\nabla \times \boldsymbol{u}(\vec{x})$$

$$\omega_x = \frac{\partial u_z}{\partial x_y}; \quad \omega_y = \frac{\partial u_z}{\partial x_x}; \quad \omega_z = \frac{1}{2}\left(\frac{\partial u_x}{\partial x_y} - \frac{\partial u_y}{\partial x_x}\right);$$

This slide shows test comparisons between accelerations and scaled rotation rates

- Fundamental Faulting Orientations & Isotropic:
  - vertical strike-slip (**SS**)
  - 45 degree dip slip (**DS**)
  - Vertical dip slip (**DD**)
  - Isotropic
- f-k reflectivity synthetics: Distance = 77 km; Depth = 6 km
- Bandpass Filter (0.01-2.5 Hz)
- The ω_3 rotations has a SH radiation pattern
- The ω_1 and ω_2 rotations have a P-SV radiation pattern
  - (ω_2 does not have the 2 (or 0.5) scale factor)
- **This allows for incorporation into the linear moment tensor inversion based on the SS, DS, DD, ISO Greens function formulation (*i.e*, synthetics are linear combination of GFs with M_{ij})**

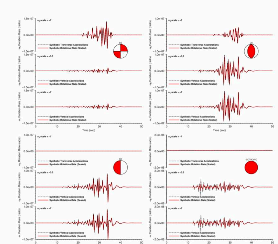

Array-Derived Rotations (Spudich et al, 1995)

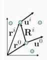

$$\mathbf{r}^i = (x_1^i, x_2^i, 0)^T \quad i = 0, 1, \ldots, N$$
$$\mathbf{u}^i = (u_1^i, u_2^i, u_3^i)^T$$
$$\mathbf{R}^i = \mathbf{r}^i - \mathbf{r}^0 \qquad \mathbf{d}^i = \mathbf{u}^i - \mathbf{u}^0$$

(podle Spudich et al., JGR, 1995) $\mathbf{d}^i = \mathbf{G}\mathbf{R}^i; \quad G_{ij} = u_{i,j}$

BASIC ASSUMPTION: uniform spatial gradients over the array !!!

$$\begin{pmatrix} d_1^i \\ d_2^i \\ d_3^i \end{pmatrix} = \begin{pmatrix} u_{1,1} & u_{1,2} & \ldots \\ u_{2,1} & u_{2,2} & \ldots \\ u_{3,1} & u_{3,2} & \ldots \end{pmatrix} \begin{pmatrix} R_1^i \\ R_2^i \\ 0 \end{pmatrix}$$

Minimum number of stations: 3

Moment Tensor Formulation

$$u_z = M_{xx}\left[\frac{ZSS}{2}\cos(2az) - \frac{ZDD}{6} + \frac{ZEP}{3}\right] + M_{yy}\left[-\frac{ZSS}{2}\cos(2az) - \frac{ZDD}{6} + \frac{ZEP}{3}\right] + M_{zz}\left[\frac{ZDD}{3} + \frac{ZEP}{3}\right] + M_{xy}[ZSS\sin(2az)] + M_{xz}[ZDS\cos(az)] + M_{yz}[ZDS\sin(az)],$$

$$u_t = M_{xx}\left[\frac{TSS}{2}\sin(2az)\right] + M_{yy}\left[-\frac{TSS}{2}\sin(2az)\right] + M_{xy}[-TSS\cos(2az)] + M_{xz}[TDS\sin(az)] + M_{yz}[-TDS\cos(az)].$$

4. Full Moment Tensor Inversion Sensitivity Results (Network Sensitivity Solutions) with and without Rotational 3-C Data

We performed MT inversions on 2- and 3-station datasets. The station referred to as the 6-C is the array with the 3-C rotation plus 3-C reference site displacement. All the single 3-C stations selected were about the same distance as the 3-C arrays. The 3-C rotational data were weighted by a factor of approx. 40 so they were the same amplitude range as the 3-C translational displacements.

Signs of MT solution improvement with rotational data:

1. **Point of highest %VR moves closer to the origin (or highest %DC).**
2. **The 80% VR contour decreases in size and covers the origin.**
3. **The 80% VR contour centered on origin rather than bi-modal distribution**

Blue – Predicted Red - Inversion

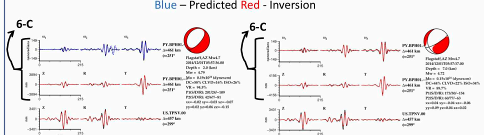

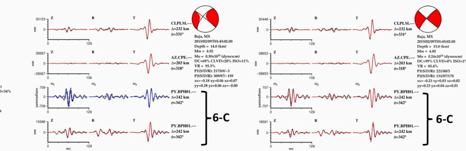

Blue – Predicted Red - Inversion